

THE ELONGATION OF SMALL CRATERS ON STEEP LUNAR SLOPES: DO POLAR VOLATILES ENHANCE ELONGATION AND MASS WASTING? Ariel N. Deutsch¹ and Valentin T. Bickel², ¹NASA Ames Research Center, Moffett Field, CA, USA (ariel.deutsch@nasa.gov), ²Center for Space and Habitability, Bern, CH.

Introduction: Understanding the distribution and abundance of volatiles cold-trapped at the poles of the Moon is a major priority for lunar science and exploration. Previously, volatiles have been interpreted to be responsible for reduced crater depths [1,2], reduced crater slopes [3], subdued topography [4,5], and mass wasting features [6,7] at high-latitude craters. Quantifying these morphometric variations in polar craters can provide important constraints on the distribution and abundance of polar ice, but doing so first requires a detailed understanding of the morphometry of lower latitude, ice-free craters.

Crater morphometry can be influenced by many factors, including the topography of the target terrain. Numerical simulations [8–10] and controlled laboratory experiments [11–13] of impacts into dry terrains demonstrate that craters tend to elongate and shallow in the direction of the slope as the angle of the target slope steepens.

In this work, we analyze the elongation of small (~20–150 meter) lunar highlands craters as a function of target slope. We compare crater statistics at lower latitudes, where surface/near-surface ice is not stable, to those at polar latitudes (including Artemis-3 candidate landing regions), where ice is stable, and discuss how volatiles may influence crater elongation/mass wasting.

Methods: *Crater elongation.* We identify small craters at lower latitudes in 2-m ortho-rectified Lunar Reconnaissance Orbiter Camera (LROC) Narrow Angle Camera (NAC) images and at polar latitudes using 5-m Lunar Orbiter Laser Altimeter (LOLA) hillshade mosaics and 2-m NAC mosaics (**Table 1**). All craters are located on local slopes $>10^\circ$. We measure their diameters down-slope (i.e., parallel to the local slope gradient) and across-slope (i.e., perpendicular to the local slope gradient) (**Fig. 1A**). The two diameters are

used to describe a crater's elongation, E , where $E = 1$ indicates a crater is symmetrical and $E > 1$ indicates a crater is elongated in the down-slope direction.

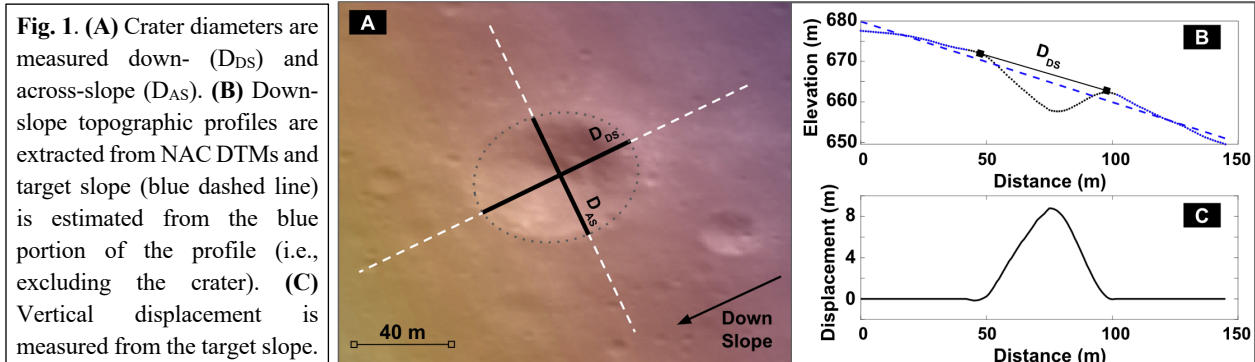
Target slope. The local slope of the terrain surrounding a given crater is used as a proxy for the target slope that existed before that crater formed. For each crater, we extract a down-slope topographic profile through the crater's center for a length of $2.5D$, where D is the crater's down-slope diameter. The crater is artificially removed from the topographic profile, a linear expression is fit across the remaining profile, and the slope of the fit is used to represent the target slope (**Fig. 1B**). Lower-latitude topography is extracted from LROC NAC Digital Terrain Models (DTMs) generated from the images used to identify the craters (pixel resolution of 2–5 m) [14] and polar topography is extracted from LOLA 5-m DEMs [15].

Crater depth. Crater depth is measured as the maximum vertical difference between the estimated local slope and the crater topography, both in the down-slope and across-slope directions (**Fig. 1C**).

Location	Topography Source	N
44°S, 129°E	NAC AUSTRVOLC	241
43°S, 285°E	NAC VINGHIRAM	64
N of Shackleton	LOLA 5M	150
*Connecting Ridge Extension	LOLA 5M	150
*Peak Near Shackleton	LOLA 5M	150

Table 1. Number of craters sampled (N) in the initial study site. *Artemis-3 candidate landing region.

Results: *Crater elongation.* Of the ~300 craters sampled at lower latitudes (**Table 1**), 55% are elongated in the downslope direction, with 21% characterized by $E > 1.1$ and 6% by $E > 1.2$. We find the proportions are higher for the 450 sampled polar craters: 70% have $E > 1$, 27% have $E > 1.1$ and 10% have $E > 1.2$. It is



possible that the presence of volatiles in polar regolith may promote downslope movement, contributing to the relatively higher proportion of elongated craters so far identified in the south polar region.

Of course, elliptical craters can also form because of oblique impacts [e.g., 16], independent of target composition or inclination. And we do identify craters elongated in a direction other than down-slope (26% of lower-latitude craters and 22% of polar craters have $E < 1$), suggesting impact conditions played a dominant role in their dimensionality.

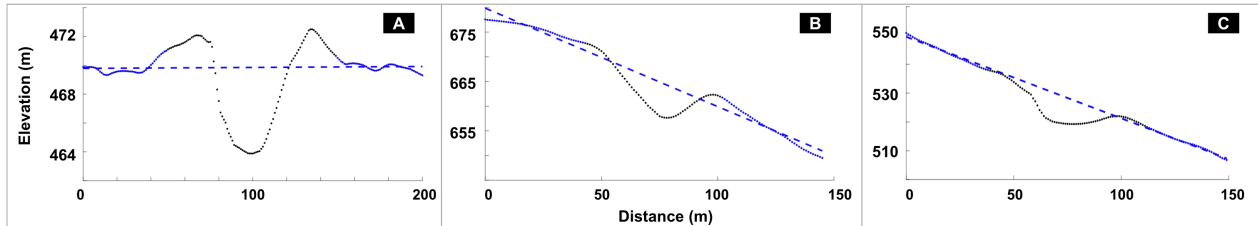


Fig. 2. Down-slope topographic profiles showing exemplary cases of (A) symmetrical craters, (B) elongated craters, and (C) broken elongated craters. As in Fig. 1, blue dashed lines represent estimated pre-existing target slope.

Crater morphometries. We find that the down-slope topographic profiles of small craters can be sorted into three primary classes: (1) Symmetrical craters have full crater rims preserved and similar down- and across-slope profiles (Fig. 2A). (2) Elongated craters have full crater rims preserved and elongated down-slope profiles (Fig. 2B). (3) Broken elongated craters lack well-preserved crater rims (Fig. 2C). Experimental work suggests there is a fourth class of craters composed of mere depressions (i.e., no identifiable rim crest morphometries) [13], but such craters are difficult to identify in the remote sensing data.

We find that as a crater becomes more elongated, the deepest part of the crater tends to shift down-slope. Additionally, the maximum vertical displacement (Fig. 1C) of elongated craters tends to be shallower when measured from down-slope profiles rather than across-slope profiles.

Work is ongoing to classify our analyzed craters and determine the correlation between target slope and the three elongation classes depicted in Fig. 2. We will place our results in context of existing models interpolating experimental data of impacts into sloped targets, which predict an elliptical crater threshold angle of 12° for the Moon [16]. We will determine whether transitions between these stages occur at the same threshold angles for polar and lower-latitude craters. If volatiles promote additional down-slope movement in small craters, then we expect the threshold angle to be slightly lower for polar craters.

Implications for polar volatiles: Here we have demonstrated that small (20–150 m) craters formed in non-level terrains often are elongated in the down-slope

direction and have relatively shallow depths, both at polar latitudes and also at lower, ice-free latitudes. Thus, it is important to consider the role of target slope on final crater shapes when using crater morphometry as a means of probing for subsurface volatiles. For example, not accounting for target slope would result in overestimating the effect of shallowing by icy infill or runout distances by icy/wet regolith. Additionally, the depths of craters formed on sloped targets could be underestimated if measuring in the down-slope direction, or if measured by extracting depths at the

geometrically central point of the crater.

However, the relatively higher proportion of elongated craters identified in polar slopes thus far suggests that perhaps volatiles do play a role in the final morphometries of small craters at the lunar poles. Future ground observations of ice abundance (e.g., via radar or neutron spectrometer) and crater morphometry would help test this hypothesis, and highly elongated craters in Artemis-3 landing regions may be prime targets.

Applications to machine learning: Work is ongoing to expand the sampling of small non-polar and polar craters. These sampling sites can be used to train a convolutional neural network to automatically detect small craters and extract morphometric and slope measurements from other NAC, Chang'e 2, and eventually ShadowCam highlands DTMs. Such a resulting larger dataset would enable more meaningful statistical comparisons between crater populations.

References: [1] Kokhanov A. et al. (2015) *SSR*, 295–302. [2] Rubanenko L. et al. (2019) *Nat Geo*, 597–601. [3] Deutsch A. et al. (2022) *LPV*, #5023. [4] Moon S. et al. (2021) *GRL*, e2020GL090780. [5] Deutsch A. et al. (2021) *PSJ*, 213. [6] Bickel V. et al. (2021) *Nat Com*, 5607. [7] Bickel V. et al. (2022) *GRL*, e2022GL099530. [8] Elbeshausen D. & Wünnemann K. (2011) *LPSC*, #1778. [9] Krohn K. et al. (2014) *PSS*, 35–56. [10] Takizawa S. & Katsuragi H. (2020) *Icarus*, 113409. [11] Aschauer J. et al. (2016) *LPSC*, #1350. [12] Aschauer J. & Kenkmann T. (2017) *Icarus*, 89–95. [13] Hayashi K. & Sumitra I. (2017) *Icarus*, 160–175. [14] Henriksen M. et al. (2020) *LSSW*, #5084. [15] <https://pgda.gsfc.nasa.gov/products/78>. [16] Bottke W. et al. (2000) *Icarus*, 108–121.